The present Chapter is structured in the following way. In Section 5.1 we present a summary of two–nucleon transfer reaction theory. It provides, together with Section 3.1 the elements needed to calculate the absolute two–nucleon transfer differential cross sections in second order DWBA, and thus to compare theory with experiment. Within this context one can, after reading this section, move directly to Chapter 6 containing examples of applications of this formalism as well as of that related to one–particle transfer processes (Ch. 4). For the practitioner in search of details and clarification we present in section 5.2 a derivation of the equations presented in section 5.1. These equations are implemented and made operative in the software COOPER used in the applications (cf. App. 6.C).

A number of Appendices are provided. Appendix 5.A briefly reminds the quantal basis for the dressing of elementary modes of excitation and of pairing interaction. In App. 5.B the derivation of first order DWBA simultaneous transfer is worked out within a formalism tailored to focus the attention on the nuclear structure correlations aspects of the process leading to effective two–nucleon transfer form factors. In App. 5.C the variety of contributions to two–nucleon transfer amplitudes (successive, simultaneous and non–orthogonality) are discussed in detail within the framework of the semi–classical approximation which provides a rather intuitive vision of the different processes. Appendices 5.D–5.G contain relations used in Sect. 5.2 as well as in the derivation of two–nucleon transfer spectroscopic amplitudes. Finally Appendix 5.H provides a glimpse of original material due to Ben Bayman[2] which was instrumental to render quantitative the studies of two-nucleon transfer, studies which can now be carried out in terms of absolute cross sections and not relative ones as done previously.

5.1 Summary of second order DWBA

Let us illustrate the theory of second order DWBA two–nucleon transfer reactions with the $A + t \rightarrow B(\equiv A + 2) + p$ reaction, in which $A + 2$ and A are even nuclei in their 0^+ ground state. The extension of the expressions to the transfer of pairs coupled to arbitrary angular momentum is discussed in subsection 5.2.10.

The wavefunction of the nucleus $A + 2$ can be written as

$$\Psi_{A+2}(\xi_A, \mathbf{r}_{A1}, \sigma_1, \mathbf{r}_{A2}, \sigma_2) = \psi_A(\xi_A) \sum_{l_i, j_i} [\phi^{A+2}_{l_i, j_i}(\mathbf{r}_{A1}, \sigma_1, \mathbf{r}_{A2}, \sigma_2)]^0_0, \qquad (5.1.1)$$

where

$$[\phi^{A+2}_{l_i, j_i}(\mathbf{r}_{A1}, \sigma_1, \mathbf{r}_{A2}, \sigma_2)]^0_0 = \sum_{nm} a_{nm} \left[\varphi^{A+2}_{n, l_i, j_i}(\mathbf{r}_{A1}, \sigma_1) \varphi^{A+2}_{m, l_i, j_i}(\mathbf{r}_{A2}, \sigma_2)\right]^0_0, \qquad (5.1.2)$$

---

section associated with the two-nucleon transfer processes between the ground state of superfluid nuclei is proportional to α_0^2 and not to Δ^2. In fact, Cooper pairs partners remain correlated even over regions in which $G = 0$, of course provided normal density is different from 0.

[2] Bayman and Kallio (1967), Bayman (1970), Bayman (1971), Bayman and Chen (1982).

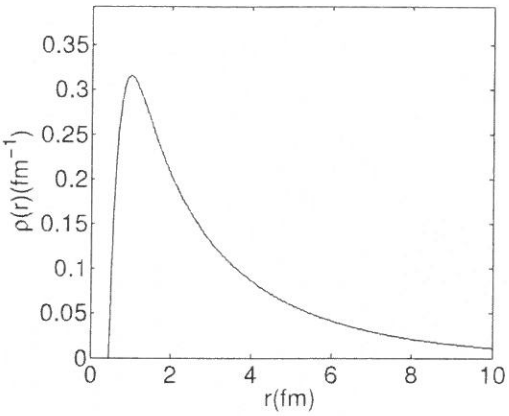

Figure 5.1.1: Radial function $\rho(r)$ (hard core 0.45 fm) entering the tritium wavefunction (cf. Tang and Herndon (1965)).

while the wavefunctions $\varphi^{A+2}_{n,l_i,j_i}(\mathbf{r})$ are eigenfunctions of a Saxon–Woods potential

$$U(r) = -\frac{V_0}{1+\exp\left[\frac{r-R_0}{a}\right]}, \qquad R_0 = r_0 A^{1/3}. \tag{5.1.3}$$

of depth V_0 adjusted to reproduce the experimental single–particles energies, together with a standard spin–orbit potential. The radial dependence of the wavefunction of the two neutrons in the triton is written as $\phi_t(\mathbf{r}_{p1}, \mathbf{r}_{p2}) = \rho(r_{p1})\rho(r_{p2})\rho(r_{12})$, where r_{p1}, r_{p2}, r_{12} are the distances between neutron 1 and the proton, neutron 2 and the proton and between neutrons 1 and 2 respectively, while $\rho(r)$ is the hard core (r_{core} = 0.45 fm) potential wavefunction depicted in Fig 5.1.1.

The two–nucleon transfer differential cross section is written as

$$\frac{d\sigma}{d\Omega} = \frac{\mu_i \mu_f}{(2\pi\hbar^2)^2}\frac{k_f}{k_i}\left|T^{(1)}(\theta) + T^{(2)}_{succ}(\theta) - T^{(2)}_{NO}(\theta)\right|^2, \tag{5.1.4}$$

where[3],

$$T^{(1)}(\theta) = 2\sum_{l_i,j_i}\sum_{\sigma_1\sigma_2}\int d\mathbf{r}_{tA} d\mathbf{r}_{p1} d\mathbf{r}_{A2}[\phi^{A+2}_{l_i,j_i}(\mathbf{r}_{A1},\sigma_1,\mathbf{r}_{A2},\sigma_2)]^{0*}_0 \chi^{(-)*}_{pB}(\mathbf{r}_{pB})$$
$$\times v(\mathbf{r}_{p1})\phi_t(\mathbf{r}_{p1},\sigma_1,\mathbf{r}_{p2},\sigma_2)\chi^{(+)}_{tA}(\mathbf{r}_{tA}), \tag{5.1.5a}$$

[3] See Bayman and Chen (1982) and App. 5.H.

is it correct ? In Fig. 3.1.1 there is a 2 instead of a 4

write in Fig. 3.1.1

gregory

gregory

Check against Eqs. in Fig. 3.1.1 p. 219

Check also with PRC Eq (38a) p. 054321 and others

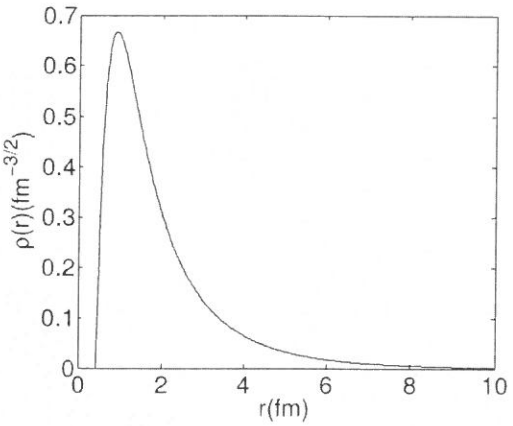

Figure 5.1.2: Radial wavefunction $\rho_d(r)$ (hard core 0.45 fm) entering the deuteron wavefunction (cf. Tang and Herndon (1965)).

Gregory

Check against formulae 3.1.1 and 3.1.2 p. 219 + 220

$$T^{(2)}_{succ}(\theta) = 2\sum_{l_i,j_i}\sum_{l_f,j_f,m_f}\sum_{\substack{\sigma_1\sigma_2\\ \sigma'_1\sigma'_2}}\int d\mathbf{r}_{dF}d\mathbf{r}_{p1}d\mathbf{r}_{A2}[\phi^{A+2}_{l_i,j_i}(\mathbf{r}_{A1},\sigma_1,\mathbf{r}_{A2},\sigma_2)]^{0*}_0\chi^{(-)*}_{pB}(\mathbf{r}_{pB})v(\mathbf{r}_{p1})$$
$$\times\phi_d(\mathbf{r}_{p1},\sigma_1)\varphi^{A+1}_{l_f,j_f,m_f}(\mathbf{r}_{A2},\sigma_2)\int d\mathbf{r}'_{dF}d\mathbf{r}'_{p1}d\mathbf{r}'_{A2}G(\mathbf{r}_{dF},\mathbf{r}'_{dF})$$
$$\times\phi_d(\mathbf{r}'_{p1},\sigma'_1)^*\varphi^{A+1*}_{l_f,j_f,m_f}(\mathbf{r}'_{A2},\sigma'_2)\frac{2\mu_{dF}}{\hbar^2}v(\mathbf{r}'_{p2})\phi_d(\mathbf{r}'_{p1},\sigma'_1)\phi_d(\mathbf{r}'_{p2},\sigma'_2)\chi^{(+)}_{tA}(\mathbf{r}'_{tA}), \tag{5.1.5b}$$

$$T^{(2)}_{NO}(\theta) = 2\sum_{l_i,j_i}\sum_{l_f,j_f,m_f}\sum_{\substack{\sigma_1\sigma_2\\ \sigma'_1\sigma'_2}}\int d\mathbf{r}_{dF}d\mathbf{r}_{p1}d\mathbf{r}_{A2}[\phi^{A+2}_{l_i,j_i}(\mathbf{r}_{A1},\sigma_1,\mathbf{r}_{A2},\sigma_2)]^{0*}_0\chi^{(-)*}_{pB}(\mathbf{r}_{pB})v(\mathbf{r}_{p1})$$
$$\times\phi_d(\mathbf{r}_{p1},\sigma_1)\varphi^{A+1}_{l_f,j_f,m_f}(\mathbf{r}_{A2},\sigma_2)\int d\mathbf{r}'_{p1}d\mathbf{r}'_{A2}d\mathbf{r}'_{dF}$$
$$\times\phi_d(\mathbf{r}'_{p1},\sigma'_1)^*\varphi^{A+1*}_{l_f,j_f,m_f}(\mathbf{r}'_{A2},\sigma'_2)\phi_d(\mathbf{r}'_{p1},\sigma'_1)\phi_d(\mathbf{r}'_{p2},\sigma'_2)\chi^{(+)}_{tA}(\mathbf{r}'_{tA}). \tag{5.1.5c}$$

The quantities $\mu_i,\mu_f(k_i,k_f)$ are the reduced masses (relative linear momenta) in both entrance (initial, i) and exit (final, f) channels, respectively. In the above expressions, $\varphi^{A+1}_{l_f,j_f,m_f}(\mathbf{r}_{A1})$ are the wavefunctions describing the intermediate states of the nucleus $F(\equiv(A+1))$, generated as solutions of a Woods-Saxon potential, $\phi_d(\mathbf{r}_{p2})$ being the the deuteron bound wavefunction (see Fig. 5.1.2). Note that some or all of the single-particle states described by the wavefunctions $\varphi^{A+1}_{l_f,j_f,m_f}(\mathbf{r}_{A1})$ may lie in the continuum (case in which the nucleus F is loosely bound or unbound). Although there are a number of ways to exactly treat such states, discretization processes may be sufficiently accurate. They can be implemented by, for example, embedding the Woods–Saxon potential in a spherical box of sufficiently large radius. In actual calculations involving e.g. the halo nucleus ^{11}Li, and where $|F\rangle = |^{10}\mathrm{Li}\rangle$,

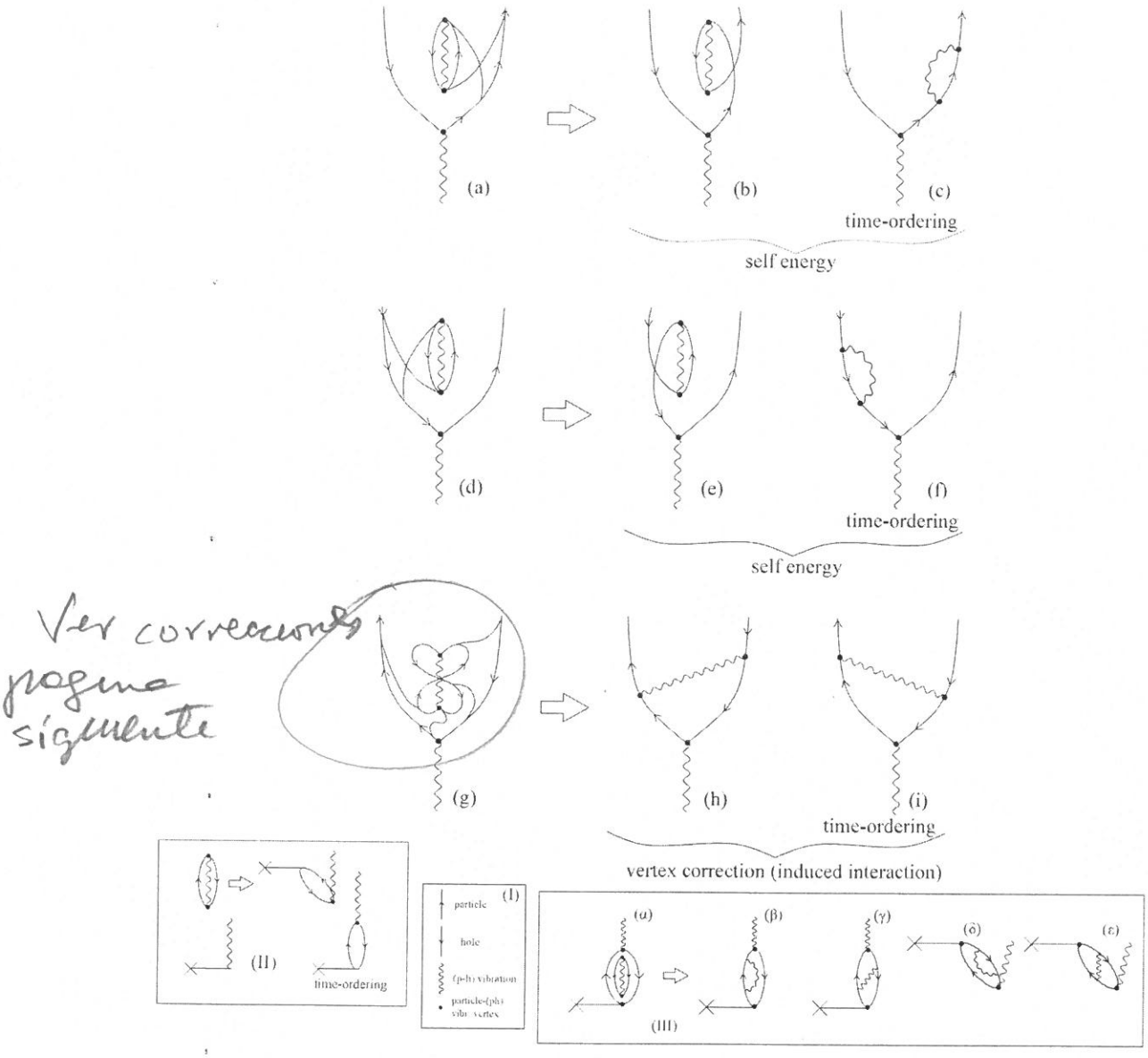

Figure 5.A.1: Nuclear field theory (NFT) diagrams describing renormalization processes associated with ZPF. For details see caption to Fig. 5.A.2.

(RPA,QRPA), and leading to the particle-vibration coupling vertex (formfactor and strength, i.e. transition density (solid dot), see inset (I), bottom). The action of an external field on the zero point fluctuations (ZPF) of the vacuum (inset (II)), forces a virtual process to become real, leading to a collective vibration by annihilating a (virtual, spontaneous) particle–hole excitation (backwards RPA Y-amplitude) or,

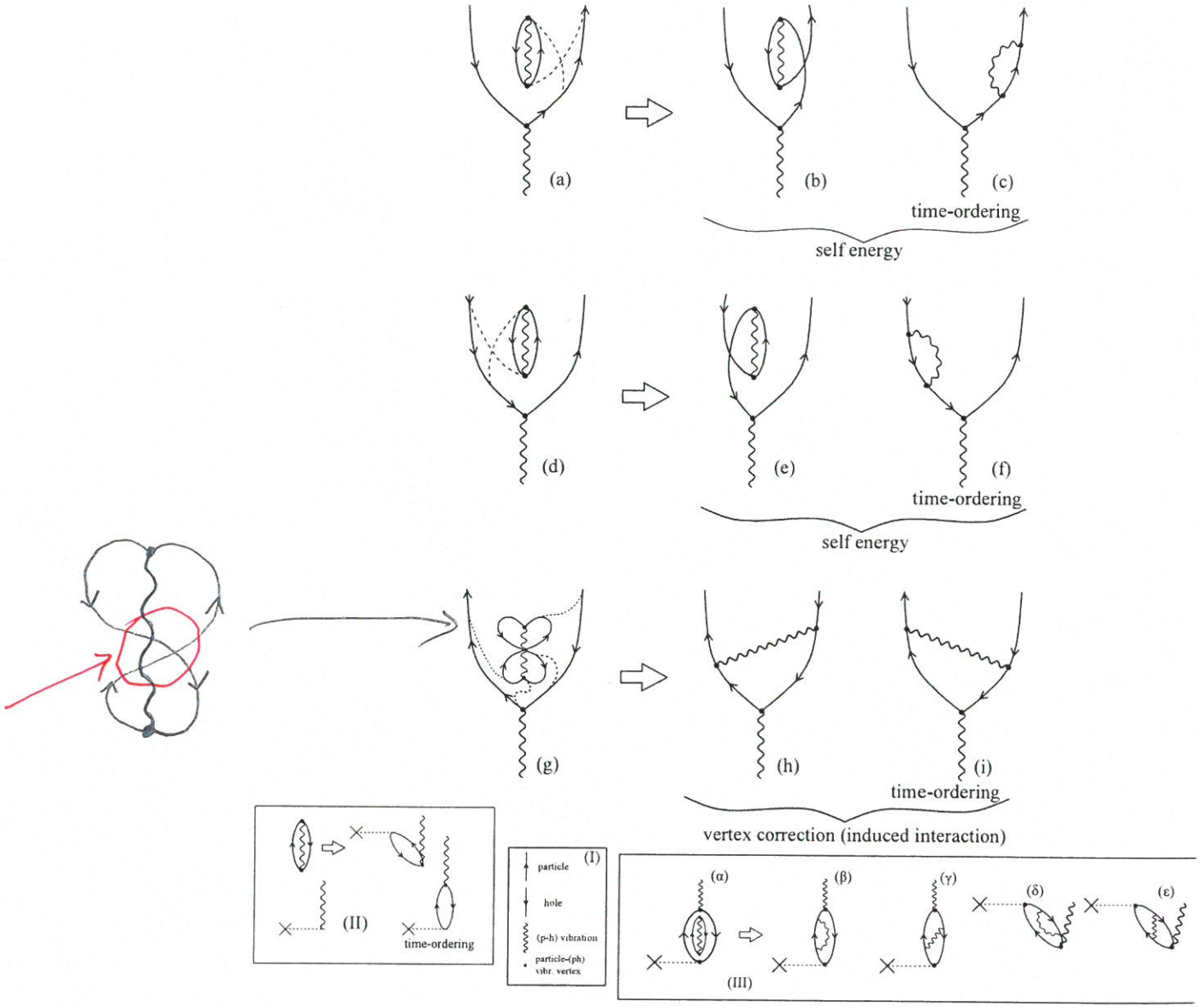

Figure 5.A.1: Nuclear field theory (NFT) diagrams describing renormalization processes associated with ZPF. For details see caption to Fig. 5.A.2.

and strength, i.e. transition density (solid dot), see inset (I), bottom). The action of an external field on the zero point fluctuations (ZPF) of the vacuum (inset (II)), forces a virtual process to become real, leading to a collective vibration by annihilating a (virtual, spontaneous) particle–hole excitation (backwards RPA amplitude) or, in the time ordered process, by creating a particle–hole excitation which even-

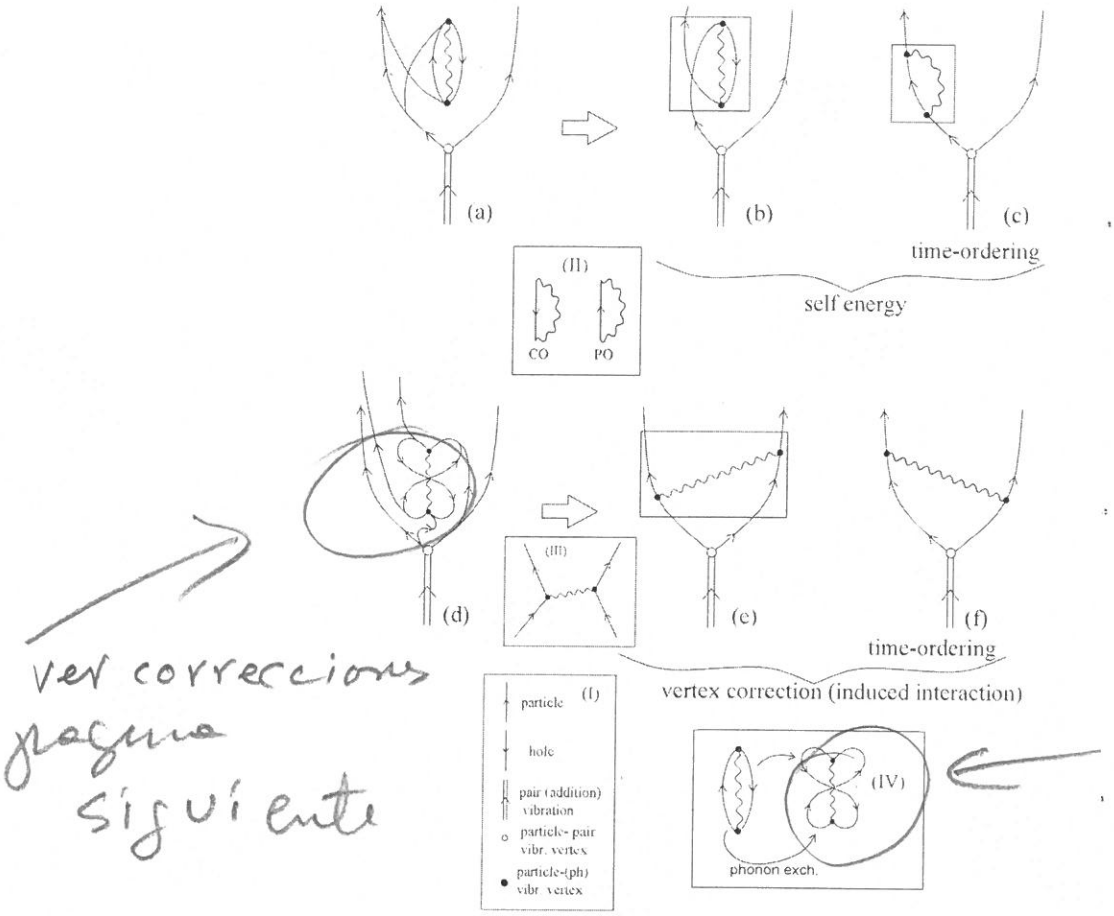

Figure 5.A.2: Pauli effects associated (p–h) ZPF dressing a pairing vibrational (pair addition) mode (see inset I) in terms of self–energy (graphs (a)–(c); correlation (CO) and polarization (PO) diagrams, inset II) and vertex correction (graphs (d)–(f); induced particle–particle (pairing) interaction) processes (inset (III)), associated with phonon exchange (inset (IV)).

in the time ordered process, by creating a particle–hole excitation which eventually, through the particle–vibration coupling vertex, correlate into the collective (coherent) state (forwardsgoing X-amplitudes). Now, oyster-like diagrams associated with the vacuum ZPF can occur at any time (see inset (III) of Fig. 5.A.1). Because the texture of the vacuum is permeated by symmetry rules (while one can violate energy conservation in a virtual state one cannot violate e.g. angular momentum conservation or the Pauli principle). The process shown in the inset III (α) leads, through Pauli principle correcting diagrams (exchange of fermionic arrowed lines) to self-energy (inset III (β), (δ)) and vertex corrections (induced $p-h$ inter-

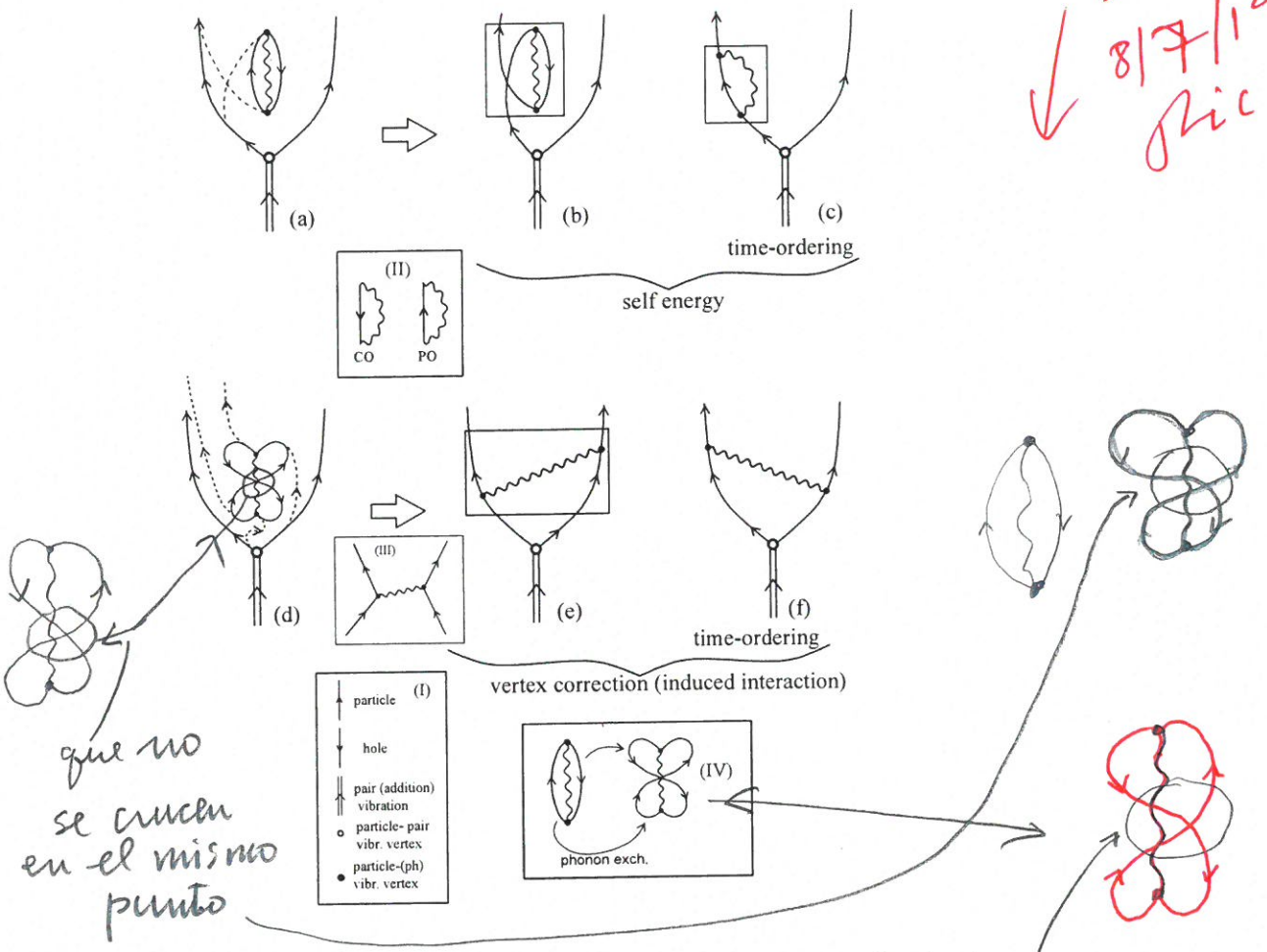

Figure 5.A.2: Pauli effects associated (p–h) ZPF dressing a pairing vibrational (pair addition) mode (see inset I) in terms of self–energy (graphs (a)–(c); correlation (CO) and polarization (PO) diagrams, inset II) and vertex correction (graphs (d)–(f); induced particle–particle (pairing) interaction) processes (inset (III)), associated with phonon exchange (inset (IV)).

tually, through the particle–vibration coupling vertex, correlate into the collective (coherent) state (forwardsgoing amplitudes). Now, oyster–like diagrams associated with the vacuum ZPF can occur at any time (see inset (III) of Fig. 5.A.1). Because the texture of the vacuum is permeated by symmetry rules (while one can violate energy conservation in a virtual state one cannot violate e.g. angular momentum conservation or the Pauli principle). The process shown in the inset III (α) leads, through Pauli principle correcting diagrams (exchange of fermionic arrowed lines) to self–energy (inset III (β), (δ)) and vertex corrections (induced p–h interaction; inset III (γ), (ε), see also graphs (h) and (i) of Fig. 5.A.1) processes (phonon ex-

$$
\begin{aligned}
T(\theta) = & \sum_{\substack{n_1 l_1 j_1 \\ n_2 l_2 j_2}} \sum_{JM_J} \sum_{nN} \sum_{S} B(n_1 l_1 j_1, n_2 l_2 j_2; J J_i J_f) \\
& \times \langle J M_J J_i M_{J_i} | J_f M_{J_f} \rangle \langle S L J | j_1 j_2 J \rangle \\
& \times \langle L M_L S M_S | J M_J \rangle \langle n0, NL, L | n_1 l_1, n_2 l_2, L \rangle \\
& \times \langle S M_S S_f M_{S_f} | S_i M_{S_i} \rangle \Omega_n \\
& \times \int d\vec{R}\, d\vec{r}_p \chi_f^{(+)*}(\vec{R}_1) \phi^*_{NLM_L}(\vec{R}) V(\rho) \phi_{000}(\vec{\rho}) \chi_i^{(+)}(\vec{R}_1),
\end{aligned}
\tag{5.B.15}
$$

where we have approximated V'_β by an effective interaction depending on $\rho = |\vec{\rho}|$.

We now define the effective two-nucleon transfer form factor as

$$
\begin{aligned}
u^{J_i J_f}_{LSJ}(R) = & \sum_{\substack{n_1 l_1 j_1 \\ n_2 l_2 j_2}} \sum_{nN} B(n_1 l_1 j_1, n_2 l_2 j_2; J J_i J_f) \langle S L J | j_1 j_2 J \rangle \\
& \langle n0, NL, L | n_1 l_1, n_2 l_2; L \rangle \Omega_n R_{NL}(R).
\end{aligned}
\tag{5.B.16}
$$

We can now rewrite eq. (5.B.15) as

$$
\begin{aligned}
T(\theta) = & \sum_{J} \sum_{L} \sum_{S} (J M_J J_i M_{J_i} | J_f M_{J_f}) (S M_S S_f M_{S_f} | S_i M_{S_i}) (L M_L S M_S | J M_J) \\
& \times \int d\vec{R}\, d\vec{r}_p \chi_p^{*(-)}(\vec{R}_2) u^{J_i J_f}_{LSJ}(R) Y^*_{LM_L} V(\rho) \phi_{000}(\vec{\rho}) \chi_i^{(+)}(\vec{R}_1).
\end{aligned}
\tag{5.B.17}
$$

Because the di–neutron has $S = 0$, we have that

$$
(L M_L 00 | J M_J) = \delta(J, L) \delta(M_L, M_J),
\tag{5.B.18}
$$

and the summations over S and L disappear from eq. (5.B.17). Let us now make also here, as done in App. 4.F, Eq. (4.F.15) for one–particle transfer reactions, the zero range approximation, that is,

$$
V(\rho) \phi_{000}(\vec{\rho}) = D_0 \delta(\vec{\rho}),
\tag{5.B.19}
$$

where D_0 is an empirical parameter ($D_0^2 = (31.6 \pm 9.3) \times 10^4$ MeV^{2}fm^2) determined to reproduce the observed absolute cross sections[20]. This means that the proton interacts with the center of mass of the di–neutron, only when they are at the same point in space. Within this approximation (cf. Fig. 5.B.1)

$$
\begin{aligned}
\vec{R} &= \vec{R}_1 = \vec{r}, \\
\vec{R}_2 &= \frac{A}{A+2} \vec{R}.
\end{aligned}
\tag{5.B.20}
$$

[20] Broglia, R.A. et al. (1973).